

## Accelerating Light Beams along Arbitrary Convex Trajectories

Elad Greenfield,<sup>1</sup> Mordechai Segev,<sup>1</sup> Wiktor Walasik,<sup>1,2</sup> and Oren Raz<sup>3</sup>

<sup>1</sup>*Physics Department and Solid State Institute, Technion, Haifa 32000, Israel*

<sup>2</sup>*Institute of Physics, Wroclaw University of Technology, 50370 Wroclaw, Poland*

<sup>3</sup>*Physics of Complex Systems, Weizmann Institute of Science, Rehovot, 76100, Israel*

(Received 19 December 2010; revised manuscript received 2 February 2011; published 25 May 2011)

We demonstrate, theoretically and experimentally, nonbroadening optical beams propagating along any arbitrarily chosen convex trajectory in space. We present a general method to construct such beams, and demonstrate it by generating beams following polynomial and exponential trajectories. We find that all such beams, accelerating along any convex trajectory, display the same universal intensity cross section, irrespective of their acceleration. The universal features of these beams are explored using catastrophe theory.

DOI: [10.1103/PhysRevLett.106.213902](https://doi.org/10.1103/PhysRevLett.106.213902)

PACS numbers: 42.25.-p

Wave packets of light propagating along arbitrarily curved trajectories in space are rapidly gaining importance. Already in the 1990s "snake beams" were proposed by Rosen and Yariv [1]. Yet, it was not until 2007 that Siviloglou and Christodoulides advanced this concept significantly further when they introduced "accelerating Airy optical beams" [2]: shape-preserving light beams whose peak intensity follows a continuous parabolic curve as they propagate in free space, just like the quantum-mechanical "Airy wave packet" [3] that inspired their invention. Optical Airy beams are now becoming of practical importance. Examples of recent applications range from optical manipulation of particles in fluids [4] to plasma-channel generation and filamentation in fluids and air [5].

Notwithstanding the recent progress [4–13] since the invention of optical Airy beams and parabolic beams, the propagation of all of these beams remains, as their name suggests, limited to parabolic trajectories in space. Indeed, constraining a light beam to be completely propagation invariant (non-diffracting) yields the Airy beam solution, which carries infinite power and propagates along a parabola [3,8,9,14]. However, this beam exists only in theory: physically, light beams carry finite power, hence in reality they must eventually broaden with propagation. Relaxing the condition of complete propagation invariance lifts the constraint on the beam trajectory: finite-energy nonbroadening accelerating beams are not theoretically constrained to propagate along parabolic trajectories. Nevertheless, the only finite-power accelerating beams thus far reported were truncated versions of the infinite-power solution, which follow a parabolic trajectory with low diffraction-broadening for finite propagation distances.

Naturally, there is a growing effort to extend the available types of nondiffracting beams: Recent advancements include a technique that can shape the intensity cross section of 3D parabolic beams [9], studies of the propagation dynamics of parabolic beams in nonlinear materials [10], introduction of spatiotemporal Airy-Bessel [11] and

Airy-Airy [12] "light bullets" exhibiting low diffraction and dispersion broadening, and generation of Airy beams in nonlinear materials with specifically engineered quasi-phase matching conditions [13]. However, families of beams accelerating along nonparabolic trajectories have not been introduced as of yet. Generation of accelerating beams which can follow any desired path in space is likely to give rise to new applications and add versatility to this emerging field.

Here, we demonstrate optical beams which accelerate along any continuous one-dimensional (1D) curve in space,  $x = f(z)$ , with the only condition being that the curve is convex. We present a general method to construct these beams, and demonstrate, theoretically and experimentally, light beams whose peak intensity accelerates along the curves  $x = z^n$ , with  $n = 1.5, 2, 3, 4, 5$ , and an "exponential beam" which follows the curve  $x = b[e^{kz} - 1]$ , with  $b$  and  $k$  positive constants. We show that all such beams, accelerating along any convex trajectory, display the same universal Airy (henceforth denoted Ai) shaped intensity cross section transverse to the propagation direction, irrespective of their acceleration. Further, the beams remain nonbroadening up to several Rayleigh lengths, and diffract strongly after the acceleration has stopped. The distance at which diffraction-broadening onsets is derived from a condition involving the beam trajectory, and the geometry of the experimental apparatus only. Last, we explore these light beams from the point of view of catastrophe optics [15], showing that all 1D convex accelerating beams comprise an optical fold catastrophe [15,16]. The universal Airy-shaped transverse intensity profile is elucidated as a characteristic of the optical fold catastrophe.

Consider the scheme sketched in Fig. 1(a). A plane wave of unit intensity, traveling in the positive  $\hat{z}$  direction, is passed through an infinitesimally thin phase mask, situated in the plane  $z = 0$ , and carrying phase distribution  $\varphi(x_0) \triangleq \varphi(x, z = 0)$ . Henceforth we denote the  $x$  coordinate in the plane  $z = 0$  as  $x_0$  [see Figs. 1(a) and 1(b) for the coordinate

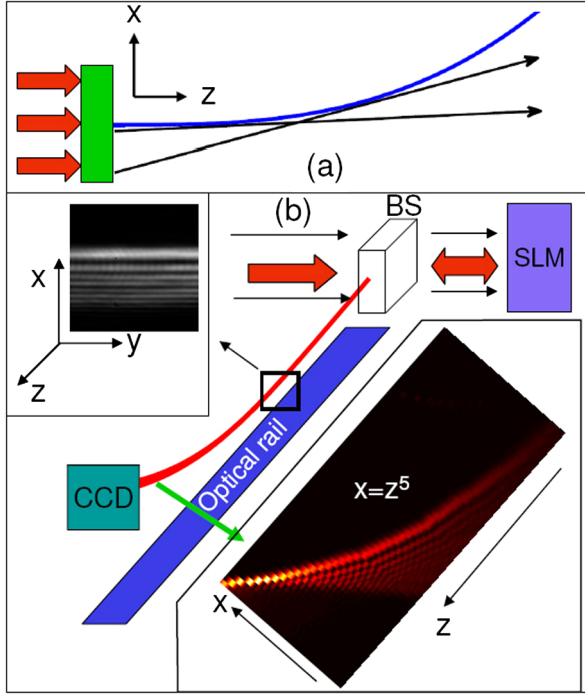


FIG. 1 (color online). Method of construction, and experimental apparatus for generation and measurement of arbitrarily accelerating optical beams. (a) Ray trajectories. A plane wave (red arrows) passes through a phase mask  $\varphi(x_0)$  (green) located at  $z = 0$ . The phase mask is obtained from Eqs. (5) and (6), and the relation  $x = f(z)$ . Following Eq. (6), the rays of light are straight lines from the mask, which are tangent to  $x = f(z)$ . As an example, two rays are presented in black. The resulting intensity distribution is propagating along the predesigned trajectory  $x = f(z)$  (blue curve). (b) Experimental apparatus (not to scale). A broad cw Gaussian beam (red arrows) is incident on a reflective spatial light modulator (SLM). The SLM (Hamamatsu LCOS-SLM) modulates the phase in the vertical ( $x$ ) direction. The beam reflected from the SLM is deflected by a beam splitter (BS), and subsequently propagates in free space above an optical rail along the  $z$  direction. A CCD camera slides along the rail and records the optical intensity in the  $x$ - $y$  plane, for several  $z$  planes along the rail. Since the images are invariant in  $y$ , we extract a single cross section along the  $x$  direction from each image. Plotting these cross sections along the  $z$  coordinates at which they were obtained, we construct an intensity cross-section in the  $x$ - $z$  plane. Top Inset: Typical experimentally recorded  $x$ - $y$  image at a given position  $z$ . Bottom Inset: Example of such an  $x$ - $z$  cross section, whose peak intensity feature follows a curve of the form  $x = az^5$ .

system]. The phase mask is finite in the  $x_0$  direction. In the paraxial ray approximation, a ray passing through the mask at  $x_0$  is deflected at an angle

$$\Theta = \partial\varphi(x_0)/\partial x_0 \quad (1)$$

with respect to the  $\hat{z}$  axis. In the Fresnel approximation, the field for any  $(x, z \geq 0)$  is

$$u(x, z) = \int \frac{1}{\sqrt{2\pi z}} e^{i\psi(x, z, x_0)} dx_0, \quad (2)$$

where  $\psi(x, z, x_0) = k(x - x_0)^2/2z + k\varphi(x_0)$ , and  $k$  is the wave number in air, and the integration is carried out over

the finite mask size. Applying the stationary-phase approximation [17] to the oscillatory integral in Eq. (2), the main contribution to  $u(x, z)$  comes from the field emanating from the stationary points on the mask,  $x_0^i$ , which fulfill  $\psi'(x_0^i) = 0$ , where “ $'$ ” hence on denotes partial differentiation with respect to  $x_0$ . These points fulfill

$$x = x_0^i + z\varphi'(x_0^i) = x_0^i + z\Theta. \quad (3)$$

These are the points on the phase mask which contribute most to the wave amplitude in Eq. (2). We approximate  $\psi$  in Eq. (2) up to the third order Taylor’s series in  $x_0$  around  $x_0^i$ , and perform straightforward integration in Eq. (2) to obtain an approximation,

$$u(x, z) \cong \sum_i B_i \text{Ai}\left(\frac{k^{2/3}(\varphi''(x_0^i) + \frac{1}{z})^2}{2^{2/3}\varphi'''(x_0^i)^{4/3}}\right). \quad (4)$$

The coefficients  $B_i$  are irrelevant to the arguments below, and are therefore presented only in the supplemental material [18].

Our goal is to set the global maximum of the optical intensity  $|u(x, z)|^2$ , in any given plane  $z$ , on the curve  $x = f(z)$ . This can be done by setting the argument of the Ai function in Eq. (4) to be exactly  $-1.019$  on every point of the curve  $x = f(z)$  [because Ai( $y$ ) has its peak at  $y = -1.019$ ]. Neglecting a small shift of the position of the maximum of the beam, we set the argument to zero instead of  $-1.019$ , obtaining a much simpler equation,

$$\varphi''(x_0^i) + \frac{1}{z} = 0. \quad (5)$$

Solving Eqs. (3) and (5) simultaneously with the relation  $x = f(z)$ , and substituting the resulting phase relation  $\varphi(x_0)$  in Eq. (2), ascertains that  $u(x, z)$  has a local maximum on the curve  $x = f(z)$ . But since the field distributes like an Ai function around this maximum, the maximum is actually a global maximum of a cross section of  $u(x, z)$  in the direction perpendicular to  $x = f(z)$ . However, this does not yet ensure that such a global maximum exists for *all* values of  $x = f(z)$ . To ensure that such a global maximum exists for all points of  $x = f(z)$ , we require that there exists a smooth, single valued, relation  $x_0(x)$  for all values of  $x$ . This way, there exist a set of points  $x_0$  (points on the initial  $z = 0$  plane) that are stationary in the integral of Eq. (2), and the fields emanating from them interfere constructively to yield the curve of global maximum intensity  $x = f(z)$ . Consequently,  $\partial x_0/\partial x$  must be single valued for all values of  $x$ . We calculate the derivative  $d\varphi'(x_0)/dx$  once through the chain rule using  $\partial x_0/\partial x$ , and a second time by directly differentiating Eq. (3). Equating the two expressions, denoting  $z = f^{-1}(x) \triangleq g(x)$ , and dropping the index  $i$  from  $x_0^i$ , (see supplemental material [18] for details), we find

$$x_0(x) = x - \frac{g}{\partial g/\partial x} = x - z \frac{\partial f(z)}{\partial z}. \quad (6)$$

Equation (6) specifies  $\Theta = \partial f(z)/\partial z$  in Eq. (3), and along with the relation  $x = f(z)$ , identifies the trajectory of the light ray leaving the mask at  $z = 0$  as a straight line from

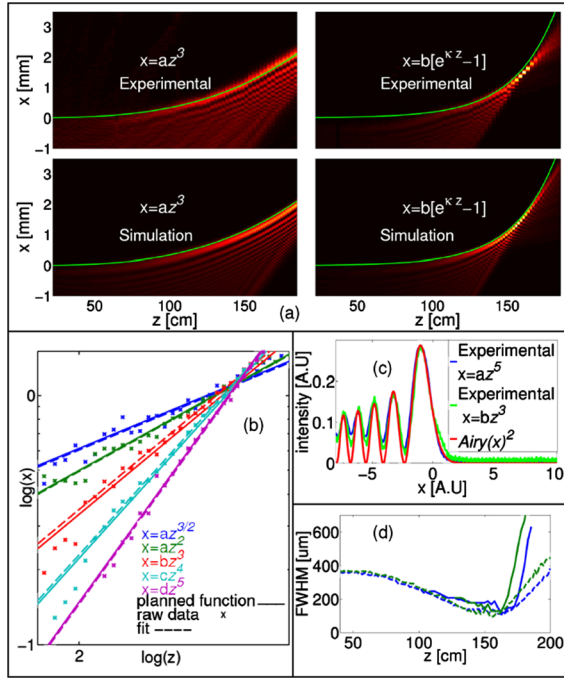


FIG. 2 (color online). Measured and simulated properties of arbitrarily accelerating optical beams. (a) Experimental (top) and simulated (bottom) optical intensity distributions for beams accelerating along the nonparabolic trajectories  $x = az^3$  and  $x = b[e^{kz} - 1]$ . The green lines are the best fits of the positions of maximum intensity of the experimental data, to these trajectories. These lines are redrawn on the simulated intensities, highlighting the agreement between theory and experiment. (b) Summary of a set of experiments of the type presented in (a) for predefined polynomial trajectories  $x = a_n z^n$  intersecting at  $z = 150$  cm. The data set for each beam is presented in a different color. The whole lines are the predefined trajectories used for calculating the masks providing the initial field phases. The “+” marks are the positions of the peaks of the experimentally-obtained intensity distribution, at each plane  $z$ . The dashed lines are best fits of these data to the predefined trajectories, the same as the green lines in (a). The data are plotted on a logarithmic scale, where the different accelerations of the beams appear as different linear slopes. (c) The  $\text{Ai}^2$ -shaped intensity pattern transverse to the propagation axis. Experimentally obtained cross sections along the  $x$  axis for the intensity distribution following the trajectories  $x = a_5 z^5$  (blue) and  $x = a_3 z^3$  (green), are compared to an  $\text{Ai}^2(x)$  function (red), in accordance with Eq. (4). (d) Experimental (whole lines) and simulated (dashed lines) full width at half maximum (FWHM) of the main-intensity feature, for beams which accelerate along the curves  $x = a_5 z^5$  (blue [dark gray]) and  $x = b[e^{kz} - 1]$  (green [medium gray]). The peak-intensity is nonbroadening, and even narrows up to  $\sim 30$  Rayleigh lengths of propagation, after which the beam abruptly starts to broaden.

(0,  $x_0$ ) which is tangent to  $f(z)$ . Figure 1(a) presents this final result schematically, showing the trajectories of two rays (black arrows) which contribute to the accelerating intensity distribution (blue line).

We offer an interpretation of our method of construction, based on optical catastrophe theory [15,16]. According to

Eq. (6), the curve  $x = f(z)$  is the envelope of rays tangent to all members of the ray family leaving the mask, and therefore a caustic [15]. Since a caustic is a manifold on which rays focus to a maximum extent, it is not surprising that the optical intensity  $|u(x, z)|^2$  has a global maximum there. The solution to the ray equation [Eq. (6)] is singular on  $x = f(z)$ : for any point below the curve  $x = f(z)$ , Eq. (6) always has exactly two solutions, corresponding to two rays that cross this point (for instance, in Fig. 1(a) the two black rays cross at some point beneath the curve). For a point which is exactly on the curve, Eq. (6) has only one solution, which is the ray tangent to the curve at that point. For a point above the curve, Eq. (6) has no solution at all, since there are no rays which are tangent to a convex curve and cross it at the same time. The configuration of critical points of the potential  $\psi$  in Eq. (2), and equivalently the number of solutions of Eq. (3), changes abruptly from 2 to 1 and then to 0 critical points on the entire caustic. This type of abrupt change in the configuration of critical points is known as a “catastrophe,” and specifically in our case—a “fold catastrophe,” the only catastrophe possible in a problem of these dimensions (the codimension is one [16]). The optical fold catastrophe is always accompanied by an  $\text{Ai}^2$ -shaped diffraction pattern near the caustic, elucidating the result of Eq. (4). Hence, all finite-power 1D beams accelerating along any convex trajectory display the same  $\text{Ai}^2$  intensity structure at the vicinity of their peak intensity, and this feature is a manifestation of a general property of the optical fold catastrophe [15,16].

We proceed to demonstrate our method experimentally. Figure 1(b) describes schematically the experimental apparatus used for generating and measuring optical beams accelerating on arbitrary convex curves. In the lower inset of Fig. 1(b), we present an example of an experimentally measured optical beam, whose peak intensity follows a curve of the form  $x = az^5$ . [“ $a$ ” and “ $b$ ” and “ $k$ ” are henceforth freely used as arbitrarily chosen constants]. Figure 2(a) (top) presents two examples of optical intensity distributions measured for beams accelerating along nonparabolic trajectories. Substituting  $x = az^3$  and  $x = b[e^{kz} - 1]$  for  $x = f(z)$  and solving Eqs. (5) and (6), we obtain phase masks  $\varphi(x_0)$  that are loaded onto the spatial light modulator (SLM). Illuminating the SLM with a plane wave, we generate light beams that propagate along these predefined curves. We measure the optical intensity in the  $x$ - $z$  plane as illustrated in Fig. 1(b). Figure 2(a) (bottom) presents results obtained by numerically simulating the experimental apparatus with the same input phase masks, using a standard beam propagation code. The experimental and the simulated optical intensities are in good agreement with each other. At  $z = 0$ , the intensity is uniform (because the SLM modulates only the phase), but as the waves propagate, intensity features appear, following the curves  $x = f(z)$ . More examples, along with a discussion of the effect of the finite size of the phase mask, are in sections B and C in the supplemental material [18].



Figure 2(b) summarizes several experiments of the type presented in Fig. 2(a). In this set of experiments, we generate a family of beams that follow the trajectories  $x = a_n z^n$ , with  $n = 1.5, 2, 3, 4, 5$ . The constants  $a_n$  are chosen such that this family of beams will intersect at  $z = 150$  cm. Evidently, the beams accelerate along their predesigned curves, and are clearly discernable from one another, demonstrating our capability to form light beams which accelerate along any convex curve  $x = f(z)$ .

We now discuss the properties of the finite-power beams accelerating along arbitrary curves. Figure 2(c) presents a cross section along the  $x$  axis [a vertical cross section of the  $x$ - $y$  image presented in Fig. 1(b)], of the experimentally obtained intensity structure of beams following the trajectories  $x = a_5 z^5$ , and  $x = a_3 z^3$ . These cross sections are compared to the square of an Airy function (red), showing good agreement. This demonstrates the prediction of Eq. (4): the diffraction pattern of a 1D accelerating beam at the vicinity of its peak intensity is always shaped like an Airy function, irrespective of the beam's acceleration, since it manifests an optical fold catastrophe. The "valleys" in the experimental data do not go down to zero as those of the theoretical Airy function, due to the crosstalk between pixels in our camera, and the imperfect efficiency of our SLM.

Turning to quantify the diffraction broadening of the beams, Fig. 2(d) presents the FWHM of the main-intensity feature, for beams accelerating along the curves  $x = a_5 z^5$  and  $x = b[e^{kz} - 1]$ , vs propagation distance  $z$ . The simulated and the measured widths are in good agreement. The peak-intensity feature for  $x = a_5 z^5$  is nonbroadening and even narrows, up to  $\sim 30$  Rayleigh lengths of propagation, at which point it abruptly starts diffracting. In the supplemental material [18], we derive an equation for the point at which diffraction onsets, show that this point is determined only by the size of the aperture and the choice of acceleration for the beam, and present additional examples.

Our method of generating accelerating beams employs a phase-only, uniform amplitude field which is launched at the plane  $z = 0$  from a finite window, whereas the Airy beams in [2] are formed by launching an Ai shaped field amplitude at the plane  $z = 0$ . The phase of our  $x \sim z^2$  beam at  $z = 0$ , coincides with the phase of the analytic expansion of the Ai function: our phase mask for the  $x \sim z^2$  beam roughly follows  $\varphi(x_0) \sim x_0^{3/2}$ , whereas asymptotically  $\text{Ai}(-x) \sim \sin(x^{3/2})$ . Notably, our beam accelerates along a parabola just like the Airy beams of [2], but its main lobe narrows instead of being invariant during propagation. This suggests that the acceleration property of finite-power accelerating beams is due only to the phase relation between the wavelets forming the beam, whereas the self-similarity feature of the peak intensity at different propagation planes can be attributed to its intensity distribution.

In this Letter, we have introduced optical beams propagating along any smooth convex trajectory in space. The equations describing the construction of these beams

provide a general platform for designing and exploring a completely new family of shaped light beams. We have shown that the beams are nonbroadening to a preplanned extent, and that their Ai<sup>2</sup> shaped diffraction pattern is a universal feature, characteristic of all arbitrarily accelerating convex 1D beams. These ideas can be used for a variety of applications. For example, our technique facilitates a means to optically move particles in air and fluid, and to use light to induce plasma channels in air, along any arbitrarily predesigned trajectories. As such, we envision that the work presented here will add both versatility and understanding to this new emerging field.

O. R. conceived the idea, O. R. and E. G. did the theory, E. G. and W. W. did the experiments, E. G. and O. R. did the analysis. M. S. provided guidance, and E. G. and M. S. wrote the Letter.

This research was supported by an Advanced Grant from the European Research Council. E. G. gratefully acknowledges the support of a Levi Eshkol Fellowship.

- 
- [1] J. Rosen and A. Yariv, *Opt. Lett.* **20**, 2042 (1995).
  - [2] G. A. Siviloglou and D. N. Christodoulides, *Opt. Lett.* **32**, 979 (2007); G. A. Siviloglou *et al.*, *Phys. Rev. Lett.* **99**, 213901 (2007).
  - [3] M. V. Berry and N. L. Balazs, *Am. J. Phys.* **47**, 264 (1979).
  - [4] J. Baumgartl, M. Mazilu, and K. Dholakia, *Nat. Photon.* **2**, 675 (2008).
  - [5] P. Polynkin, M. Kolesik, and J. Moloney, *Phys. Rev. Lett.* **103**, 123902 (2009); P. Polynkin *et al.*, *Science* **324**, 229 (2009).
  - [6] G. A. Siviloglou *et al.*, *Opt. Lett.* **33**, 207 (2008).
  - [7] M. Mazilu *et al.*, *Laser Photon. Rev.* **4**, 529 (2010); Y. Kaganovsky and E. Heyman, *Opt. Express* **18**, 8440 (2010); L. Carretero *et al.*, *Opt. Express* **17**, 22432 (2009); H. I. Sztul and R. R. Alfano, *Opt. Express* **16**, 9411 (2008); P. Saari, *Opt. Express* **16**, 10303 (2008).
  - [8] M. A. Bandres, *Opt. Lett.* **34**, 3791 (2009).
  - [9] S. Lopez-Aguayo *et al.*, *Optics and Photonics News* **21**, 43 (2010); S. Lopez-Aguayo *et al.*, *Phys. Rev. Lett.* **105**, 013902 (2010).
  - [10] Y. Hu *et al.*, *Opt. Lett.* **35**, 3952 (2010).
  - [11] A. Chong *et al.*, *Nat. Photon.* **4**, 103 (2010).
  - [12] D. Abdollahpour *et al.*, *Phys. Rev. Lett.* **105**, 253901 (2010).
  - [13] T. Ellenbogen *et al.*, *Nat. Photon.* **3**, 395 (2009).
  - [14] K. Unnikrishnan and A. R. P. Rau, *Am. J. Phys.* **64**, 1034 (1996).
  - [15] C. Upstill and M. V. Berry, *Catastrophe Optics: Morphologies of Caustics and their Diffraction Patterns* (North-Holland, New York, 1980), Vol. XVIII.
  - [16] P. T. Saunders, *An Introduction to Catastrophe Theory* (Cambridge University Press, Cambridge England; New York, 1980), pp. xii.
  - [17] V. Guillemin and S. Sternberg, *Geometric Asymptotics* (American Mathematical Society, Providence, R.I., 1977), pp. xviii.
  - [18] See supplemental material at <http://link.aps.org/supplemental/10.1103/PhysRevLett.106.213902> for derivations of the equations and further examples.